Simple analytical model for high-partial-wave ultracold molecular collisions

Yan-Peng Bai,[1] Jing-Lun Li,[1,2] Gao-Ren Wang,[1,*] Zhong-Bo Chen,[1] Bo-Wen Si,[1] and Shu-Lin Cong[1,†]
[1]*School of Physics, Dalian University of Technology, Dalian 116024, China*
[2]*Eindhoven University of Technology, P. O. Box 513, 5600 MB Eindhoven, The Netherlands*

(Received 10 January 2020; revised manuscript received 29 April 2020; accepted 11 May 2020; published 2 June 2020)

The investigation of ultracold atomic or molecular collision is important for us to understand the essence of a chemical reaction. We present a simple analytical model of arbitrary-order partial-wave scatterings for ultracold molecular collision in the threshold regime. The threshold formulas of the transmission and reflection coefficients are given. For high-partial-wave collision, shape resonance will take place because of the existence of a centrifugal barrier. We investigate the effect of shape resonance and short-range interaction on molecular collisions. Moreover, we find a method to fit the loss parameter from the experimental data of ultracold bosonic molecular collision. As an applied example, we calculate the thermally average loss rate for the ultracold ^{87}Rb ^{133}Cs + ^{87}Rb ^{133}Cs collision, our results are consistent with the recent experimental and theoretical results of Gregory *et al.* [Nat. Commun. **10**, 3104 (2019)].

DOI: 10.1103/PhysRevA.101.063605

I. INTRODUCTION

Recently, ultracold molecular collision has attracted much attention from researchers due to its pronounced quantum effect and excellent controllability [1–6]. Ultracold reactants can be precisely prepared in some defined quantum states [7–12]. The probe technique of hypefine states of reaction products has also made great progress [13,14]. Meanwhile, new theoretical methods have been developed [15,16]. The investigation of ultracold molecular collision can help us understand the essence of a chemical reaction.

Ospelkaus *et al.* indicated that the chemical reaction rate is strongly influenced by the long-range interaction [17]. The discrepancy of the rate coefficient obtained by theory and experiment in ultracold ^{23}Na ^{40}K + ^{40}K collision in different hyperfine states suggests that the short-range interaction should be considered [18]. Both short-range and long-range interactions are equally important for molecular collision [19,20]. In addition, the formation of long-lived complexes in the short-range region also has an influence on loss rate [21–24]. For the collision pairs with a very small reactivity, the reaction rate is close to zero. At ultralow temperatures, however, the reaction rate can be dramatically enhanced by the shape resonance due to tunneling through the centrifugal barrier, although the reactivity is small [25–28]. For high-partial-wave collision, the shape resonance will take place due to the presence of quasibound states behind the centrifugal barrier. The calculation of Sakimoto suggested that the reaction probability approaches unity which is attributed to the shape resonance [29]. The shape resonance is closely related to short-range interaction. Both short-range interaction and shape resonance have some influence on molecular loss rate, but the relation between them is rather complicated and needs to be further clarified. In our previous work [30], we investigated theoretically the *s*-wave molecular collision reaction. For the *s*-wave molecular collision, there is no shape resonance. Here, we present a simple analytical model of arbitrary-order partial-wave scatterings for ultracold molecular collision in the threshold regime in order to study the effect of shape resonance on loss rate and simulate the recent experiments of ultracold molecular collision more accurately [31,32]. The short-range physics is characterized by a loss parameter. The threshold formulas of reflection and transmission coefficients are derived. Our theoretical model can be used to fit accurately experimental data. As an applied example, the loss rate of ^{87}Rb ^{133}Cs molecules in the ^{87}Rb ^{133}Cs + ^{87}Rb ^{133}Cs collision is calculated, and the fitting loss parameter y is given.

The paper is organized as follows. In Sec. II, we present the transmission and reflection coefficients for arbitrary-order partial-wave scatterings. In Sec. III, we discuss the influence of shape resonance and short-range interaction on molecular loss rate. And an applied example for ultracold molecular collision is given. Finally, a conclusion is drawn in Sec. IV.

II. THEORY

The radial Schrödinger equation describing particle collision is given by

$$\left(-\frac{d^2}{dR_s^2}+\frac{L(L+1)}{R_s^2}+V(R_s)-E_s\right)\psi(R_s)=0, \quad (1)$$

where $R_s = R/\beta_\alpha$ is the scaled radius, $E_s = E/s_E$ is the scaled energy, and L is the relative orbital angular momentum quantum number. The length scale β_α is defined as $\beta_\alpha = (2\mu C_\alpha/\hbar^2)^{1/(\alpha-2)}$ with μ being the reduced mass, and the energy scale is $s_E = \hbar^2/(2\mu\beta_\alpha^2)$. The potential is given by $V(R_s) = -1/R_s^\alpha$ with $\alpha > 2$ being a positive integer.

*gaoren.wang@dlut.edu.cn
†shlcong@dlut.edu.cn

At nonzero collision energy, there are two sets of asymptotic solutions for Eq. (1),

$$f^{o\pm} = \frac{e^{i\pi/4}}{\sqrt{\pi k_s}} e^{\pm i k_s R_s}, \tag{2}$$

in the long-range region of $R_s \gg 1$ and

$$f^{i\pm} = \frac{e^{i\pi/4}}{\sqrt{\pi k_s}} \exp\left(\pm i \int_{R_m}^{R_s} k_s dR_s'\right), \tag{3}$$

in the short-range region of $R_s \ll 1$, where $k_s = \sqrt{E_s - V(R_s') - L(L+1)/R_s'^2}$ and R_m is a reference point that determines the phases of $f^{i\pm}$ [30,33–35]. These solutions can be used to define the traveling wave going inside-out ψ^{io} and the traveling wave going outside-in ψ^{oi} in the long-range region,

$$\begin{pmatrix} \psi^{io} \\ \psi^{oi} \end{pmatrix} \overset{R_s \gg 1}{=} \begin{pmatrix} t^{io} & 0 \\ r^{oi} & 1 \end{pmatrix} \begin{pmatrix} f^{o+} \\ f^{o-} \end{pmatrix}, \tag{4}$$

and in the short-range region,

$$\begin{pmatrix} \psi^{io} \\ \psi^{oi} \end{pmatrix} \overset{R_s \ll 1}{=} \begin{pmatrix} 1 & r^{io} \\ 0 & t^{oi} \end{pmatrix} \begin{pmatrix} f^{i+} \\ f^{i-} \end{pmatrix}, \tag{5}$$

where $r^{io}(r^{oi})$ and $t^{io}(t^{oi})$ are the reflection and transmission coefficients corresponding to the traveling wave going inside out (outside in) [30,33–35].

At zero collision energy, two linearly independent solutions for Eq. (1) can be expressed in the Bessel functions as

$$\psi_1(R_s) = \sqrt{R_s} J_\nu(z), \quad \psi_2(R_s) = \sqrt{R_s} J_{-\nu}(z), \tag{6}$$

where $\nu = (2L+1)/(\alpha-2)$ and $z = 2/(\alpha-2) R_s^{(2-\alpha)/2}$. When $E_s \to 0$, we rewrite ψ^{io} and ψ^{oi} in terms of zero-energy solutions as

$$\begin{pmatrix} \psi^{io} \\ \psi^{oi} \end{pmatrix} \overset{E_s \to 0}{=} \mathbf{C} \begin{pmatrix} \psi_1 \\ \psi_2 \end{pmatrix} = \begin{pmatrix} c_{11} & c_{12} \\ c_{21} & c_{22} \end{pmatrix} \begin{pmatrix} \psi_1 \\ \psi_2 \end{pmatrix}, \tag{7}$$

where the energy-dependent matrix $\mathbf{C}$ is given in the Appendix [36,37]. Using Eqs. (4) and (5), we straightforwardly get the transmission and reflection coefficients of partial-wave L,

$$t^{io} = t^{oi} = \frac{2\sqrt{\pi}(\alpha-2)^{-\nu-1/2}}{\Gamma(1+\nu)(2L+1)!!} \frac{k_s^{L+1/2} e^{-iL\pi/2}}{f(k_s) e^{-i(z_m - \pi/4 + \nu\pi/2)} + e^{-i(z_m - \pi/4 - \nu\pi/2)}}, \tag{8}$$

$$r^{io} = \frac{f(k_s) e^{i(z_m - \pi/4 + \nu\pi/2)} + e^{i(z_m - \pi/4 - \nu\pi/2)}}{f(k_s) e^{-i(z_m - \pi/4 + \nu\pi/2)} + e^{-i(z_m - \pi/4 - \nu\pi/2)}}, \tag{9}$$

$$r^{oi} = \frac{f(k_s) - e^{i\nu\pi}}{f(k_s) + e^{i\nu\pi}} e^{-iL\pi}, \tag{10}$$

with

$$f(k_s) = c_{11}/c_{12} = i\Gamma(1-\nu) k_s^{2L+1} / [\Gamma(1+\nu)(\alpha-2)^{2\nu} \times (2L+1)!!(2L-1)!!], \tag{11}$$

where $\Gamma(x)$ is the Γ function. z_m is the value of z at R_m, which can be taken to be any value and has no effect on final results. We here take z_m to be $\pi/4$ as Gao did [33]. The derivation of Eqs. (8)–(10) is given in the Appendix. It is noted that Eqs. (8)–(10) are low-energy expansions of reflection and transmission coefficients.

The short-range interaction is contained in the matrix $S^c = e^{i2\delta^s} e^{i2(-z_m + \pi/4)}$ [30,38] and the loss parameter y [25,39–42]. The short-range phase-shift δ^s is related to the scattering length,

$$\frac{a}{\bar{a}} = \frac{1}{\cos \nu_0 \pi} \frac{\tan \delta^s + \tan \frac{\nu_0 \pi}{2}}{\tan \delta^s - \tan \frac{\nu_0 \pi}{2}}, \tag{12}$$

where $\nu_0 = 1/(\alpha-2)$ and $\bar{a}$ is the mean scattering length [43]. The S matrix can be expressed as [25,33]

$$S_L = (-1)^{L+1} \left[r^{oi} + \frac{t^{oi} \zeta S^c t^{io}}{1 - r^{io} \zeta S^c} \right], \tag{13}$$

where $\zeta = (1-y)/(1+y)$.

The partial-wave loss rate $K_L = s_K K_{Ls}$, elastic collision rate $K_L^{\rm el} = s_K K_{Ls}^{\rm el}$, and thermally average loss rate $\mathcal{K}(T) = s_K \mathcal{K}_s(T_s)$ are written in dimensionless forms as

$$K_{Ls} = \frac{g}{k_s}(2L+1)(1 - |S_L|^2), \tag{14}$$

$$K_{Ls}^{\rm el} = \frac{g}{k_s}(2L+1)|1 - S_L|^2, \tag{15}$$

$$\mathcal{K}_s(T_s) = \frac{2}{\sqrt{\pi}} T_s^{-3/2} \int_0^\infty E_s^{1/2} e^{-E_s/T_s} K_s dE_s, \tag{16}$$

where $s_K = \pi\hbar\beta_\alpha/\mu$ is the scaled unit of loss rate and $g = 1$ for distinguishable particles and $g = 2$ for identical particles in the same internal state. $T_s = T/s_T$ is the scaled temperature, where $s_T = s_E/k_B$ is the scaled temperature unit with k_B being the Boltzmann constant. The total loss rate is $K = s_K K_s = s_K \sum_L K_{Ls}$, and the total elastic collision rate is $K^{\rm el} = s_K K_s^{\rm el} = s_K \sum_L K_{Ls}^{\rm el}$.

III. RESULTS AND DISCUSSIONS

For the hard-core plus $-1/R_s^6$ potential, moduli and phases of reflection and transmission coefficients for $L = 1$–4 are plotted in Figs. 1(a)–1(c). The black solid lines, red dashed lines, blue dotted lines and orange short dot-dashed lines are calculated by the threshold formulas [Eqs. (8)–(10)], and the black dot-dashed lines, red double dot-dashed lines (squares),

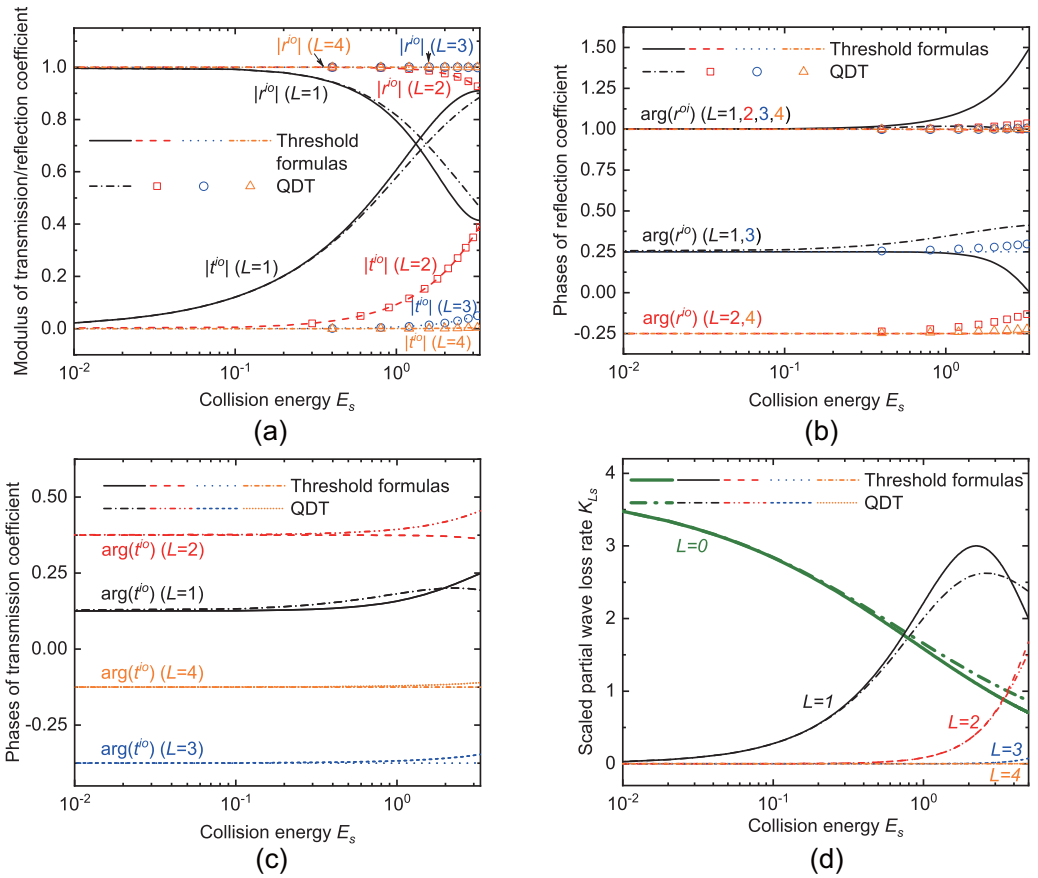

FIG. 1. (a) Modulus of transmission and reflection coefficients for $L = 1-4$ calculated by the threshold formulas (the black solid lines, red dashed lines, blue dotted lines and orange short dot-dashed lines represent partial-waves $L = 1-4$, respectively.) and quantum defect theory (QDT) (the black dot-dashed lines, red double dot-dashed lines (squares), blue short dashed lines (circles) and orange short dotted lines (triangles) represent $L = 1-4$, respectively.). E_s is the scaled energy and is dimensionless. Since the moduli of both r^{io} (t^{io}) and r^{oi} (t^{oi}) are equal, we use $|r^{io}|$ ($|t^{io}|$) to denote their moduli. (b) and (c) Phases of transmission and reflection coefficients with units of π for $L = 1-4$ calculated by the threshold formulas and QDT. The phases of t^{io} and t^{oi} are equal, thus, we use arg(t^{io}) to denote their phases. (d) Scaled partial wave loss rate K_{Ls} as a function of E_s for the universal reaction. The thick green solid (dot-dashed) line represents K_{Ls} for $L = 0$ calculated by the threshold formulas (QDT).

blue short dashed lines (circles) and orange short dotted lines (triangles) are calculated by the QDT [33,44]. In Fig. 1, the black, red, blue, and orange lines show the calculated results for $L = 1$–4, respectively. The case for $L = 0$ was discussed in our previous paper [30]. As shown in Fig. 1(a), when $E_s < 1$, the moduli of r^{io} (r^{oi}) and t^{io} (t^{oi}), calculated by using the threshold formulas for $L = 1$, agree well with those by using the QDT. For $L = 2$–4, the results calculated by the two methods are almost identical within the given energy range in Fig. 1(a). In Figs. 1(b) and 1(c), the phases calculated by the threshold formulas are consistent with those calculated by the QDT when $E_s < 1$. In the threshold regime, the phases of r^{oi} are π for $L = 1$–4, the phases of r^{io} are $\pi/4$ for $L = 1$ and 3, $-\pi/4$ for $L = 2$ and 4, the phase of t^{io} (t^{oi}) is $\pi/8$ for $L = 1$, $3\pi/8$ for $L = 2$, $-3\pi/8$ for $L = 3$, and $-\pi/8$ for $L = 4$. The scaled loss rates of partial-waves $L = 0$–4 for the universal reaction ($y = 1$) are shown in Fig. 1(d). The loss rate for the s-wave collision converges to $\pi/\Gamma(5/4)^2$ as $E_s \to 0$ [30]. In Fig. 1(d), the thick green dot-dashed line, black dot-dashed line, red double dot-dashed line, blue short dashed line and orange short dotted line show the partial-wave loss rates calculated by the QDT for $L = 0-4$, respectively. It can be seen that the results calculated by the threshold formulas are essentially consistent with those by the QDT when $E_s < 3$.

When $E_s \to 0$, the partial-wave loss rates as a function of δ^s and y are plotted in Figs. 2(a)–2(e) where the finite range $0 \leqslant \delta^s < \pi$ corresponds to infinite range of scattering length $-\infty < a < \infty$. As shown in Figs. 2(a)–2(e), the peaks appear around $\delta^s = \pi/8$ for $L = 0$ and 4, $\delta^s = 3\pi/8$ for $L = 1$, $\delta^s = 5\pi/8$ for $L = 2$, and $\delta^s = 7\pi/8$ for $L = 3$. These peaks can be regarded as the results of the quantum coherent superposition of different reflection paths [33,44]. In Eq. (14), the loss probability $P_L = 1 - |S_L|^2$ can be expressed as [33,44]

$$P_L = 1 - |S_L|^2 = |\sqrt{1-\zeta^2}t^{oi}[1 + r^{io}\zeta S^c + (r^{io}\zeta S^c)^2 + \cdots + (r^{io}\zeta S^c)^n + \cdots]|^2. \quad (17)$$

When $z_m = \pi/4$, S^c in Eq. (17) is equal to $S^c_{\rm eff}$ in Ref. [44]. It is noted that a phase difference $\theta_L = \arg(r^{io}S^c)$,

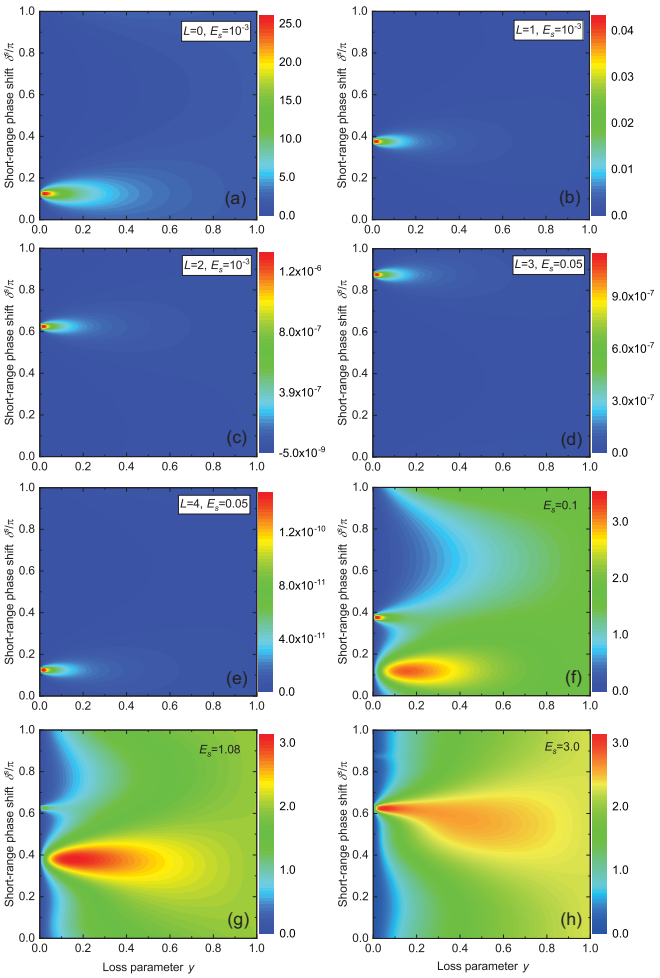

FIG. 2. (a)–(e) Scaled partial-wave loss rate K_{Ls} as a function of y and δ^s with $E_s = 0.001$ for $L = 0$–2 and $E_s = 0.050$ for $L = 3$ and 4. (f)–(h) Scaled total loss rate K_s as a function of y and δ^s for $E_s = 0.10,\ 1.08,$ and 3.00.

where $0 \leqslant \theta_L < \pi$ exists between the adjacent terms in the square brackets in Eq. (17). Obviously, the peaks in Figs. 2(a)–2(e) correspond to the maxima of loss probability P_L, which requires the phase difference $\theta_L = 0$.

We now calculate θ_L in the threshold regime. As $k_s \to 0$, the reflection coefficient r^{io} in Eq. (9) reduces to $r^{io} = [1 + i2f(k_s)\sin\nu\pi]e^{-i\nu\pi}$, where $1 + i2f(k_s)\sin\nu\pi$ is real and positive. Thus, the phase difference θ_L is given by

$$\theta_L = \arg(r^{io}S^c) = 2\delta^s - \nu\pi. \tag{18}$$

Let $\theta_L = 0$, yielding $\delta^s = \nu\pi/2 = L\pi/4 + \pi/8$ with a period of π for partial-waves $L = 0$–3, ... [45,46]. These values just correspond to the peaks in Figs. 2(a)–2(e). Due to the centrifugal barrier for $L > 0$, the zero-energy quasibound state exists, and the shape resonance will take place.

The total loss rates as a function of δ^s and y when $E_s = 0.10,\ 1.08$ and 3.00 are plotted in Figs. 2(f)–2(h). When $E_s = 0.10$, a small promontory appears around $\delta^s = 3\pi/8$, which is caused by the shape resonance. This indicates that a quasibound state of partial-wave $L = 1$ exists and is very close to the threshold [45,46]. When $E_s = 1.08,$ and 3.00, there is also a small promontory around $\delta^s = 5\pi/8$ for $L = 2$, $\delta^s = 7\pi/8$ for $L = 3$. In addition, the peak around $\delta^s = \pi/8\ (3\pi/8, 5\pi/8)$ for $E_s = 0.10\ (1.08, 3.00)$ can be also observed. We note that the shape resonance takes place only if $y \to 0$, indicating that the shape resonance plays an important role in the collision system with a very small reactivity [47]. As Gao pointed out [33,44], the shape resonance results from the coherent superposition of reflection paths when a quasibound state exists. The coherent superposition of reflection paths can change the loss rate.

For the elastic collision, $|1 - S_L|^2$ in Eq. (15) can be expressed as [33,44]

$$|1 - S_L|^2 = |1 + e^{iL\pi}\{r^{oi} + t^{oi}\zeta S^c t^{io}[1 + r^{io}\zeta S^c + (r^{io}\zeta S^c)^2 + + \cdots + (r^{io}\zeta S^c)^n \cdots]\}|^2. \tag{19}$$

When $k_s \to 0$, the transmission coefficients t^{oi} and t^{io} are proportional to $k_s^{L+1/2}e^{-i(\nu+L)\pi/2}$, and the reflection coefficient r^{oi} reduces to $r^{oi} = [-1 + 2f(k_s)e^{-i\nu\pi}]e^{-iL\pi}$. Substituting the threshold formulas of t^{oi}, t^{io}, r^{oi}, and r^{io} into Eq. (19), we can obtain that the elastic collision rate also reaches its maximum

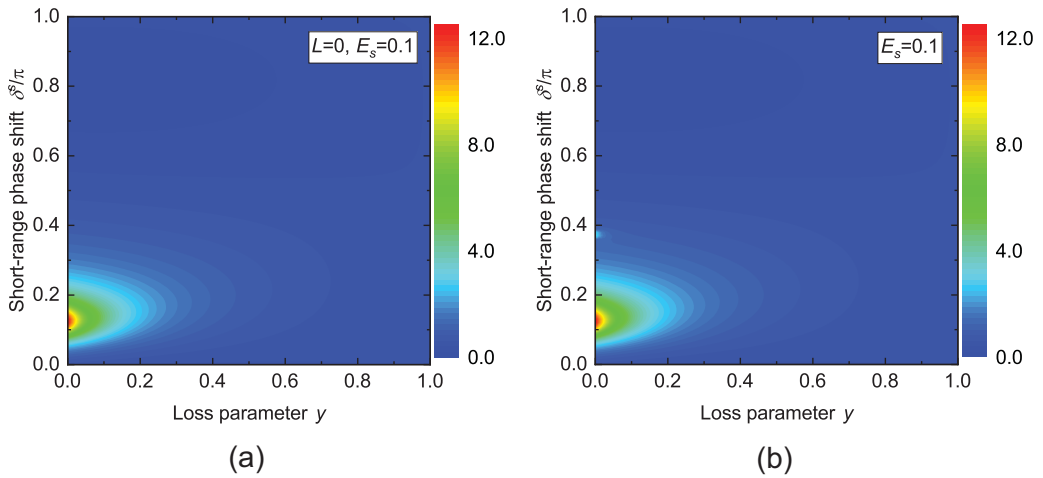

FIG. 3. (a) Scaled partial-wave elastic collision rate $K_{Ls}^{\rm el}$ as a function of y and δ^s. (b) Scaled total elastic collision rate $K_{Ls}^{\rm el}$ as a function of y and δ^s. Scaled energy $E_s = 0.10$.

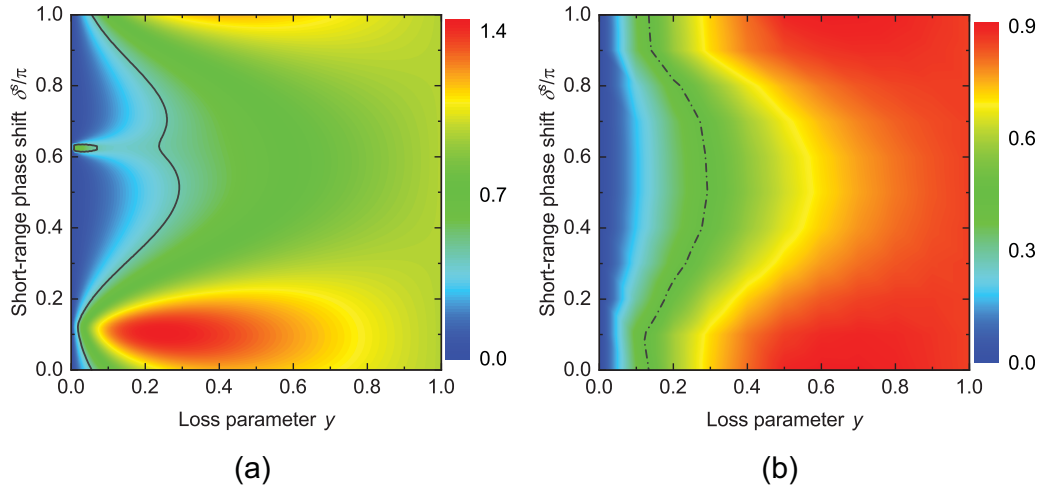

FIG. 4. (a) Thermally average loss rate $\mathcal{K}(T)$ at $T = 1.5\ \mu$K as a function of y and δ^s for ^{87}Rb ^{133}Cs + ^{87}Rb ^{133}Cs collision. The black solid line represents the measured value of $\mathcal{K}_{\rm exp} = 0.44$ in experiment [32]. (b) The change in $\mathcal{K}_{\rm min}$ with y and δ^s. The black dot-dashed line shows the range of y. Units of $\mathcal{K}(T)$ and $\mathcal{K}_{\rm min}$ are both 10^{-10} cm^3/s.

at $\delta^s = L\pi/4 + \pi/8$. For the s wave, a peak of the elastic collision rate is located at $\delta^s = \pi/8$ as shown in Fig. 3(a). The total elastic collision rate is plotted in Fig. 3(b) where a small promontory appears at $\delta^s = 3\pi/8$ due to the p-wave shape resonance.

As an application of our model, we calculate the thermally average loss rate $\mathcal{K}(T)$ for ^{87}Rb ^{133}Cs + ^{87}Rb ^{133}Cs collision at $T = 1.5\ \mu$K corresponding to $T_s = 0.45$ as shown in Fig. 4 (a). The peak of $\mathcal{K}$ around $\delta^s = \pi/8$ is mainly attributed to the loss rate of the s-wave collision. A small promontory around $\delta^s = 5\pi/8$ is caused by the d-wave shape resonance. As in the above analysis, both the peak at $\delta^s = \pi/8$ and the promontory at $\delta^s = 5\pi/8$ always correspond to the situation of $\theta_L = 0$ where the superposition of different paths leads to the loss rate reaching its maximum. The black solid line in Fig. 4(a) shows the experimental value of 0.44×10^{-10} cm^3/s [32].

As shown in Fig. 1(a), the loss rate of the s-wave collision dominates at low collision energy, and the loss rate of the high-partial wave dominates at high collision energy. Because of the contribution of different partial waves to the total loss rate and the effect of temperature, a minimum $\mathcal{K}_{\rm min}$ appears in the thermally average loss rate [44]. $\mathcal{K}_{\rm min}$ changes with y and δ^s. Using a pair of δ^s and y, we can find a $\mathcal{K}_{\rm min}$ in the curve of $\mathcal{K}(T)$. By scanning all the values of y from 0 to 1 and δ^s from 0 to π, the change in $\mathcal{K}_{\rm min}$ with y and δ^s is given in Fig. 4(b). For a fixed y, $\mathcal{K}_{\rm min}$ changes with δ^s with a period of π. For a fixed δ^s, $\mathcal{K}_{\rm min}$ increases monotonously with y. The dashed-dotted line in Fig. 4(b) corresponds to the minimal thermally average loss rate of 0.44×10^{-10} cm^3/s measured in experiment [32]. Thus, all the possible values of y are distributed around the dashed-dotted line. From the experimental data [32], we find the best-fitting result to be $y = 0.27$ and $\delta^s = 0.62\pi$. Compared with the fitting values of Gregory *et al.* using the QDT, $y = 0.26$ and $\delta^s = 0.56\pi$ [32], the difference in y is 0.01 and that in δ^s is 0.06π, and the difference in the scattering length is $44.59a_0$, where a_0 is the Bohr radius. Our theoretical results are consistent with those calculated by using the QDT [32]. This indicates that the threshold laws of reflection and transmission coefficients are precise for studying ultracold molecular collision. In fact, the result in Fig. 4(b) can be applied to other bosonic systems, only s_K being different. The calculation of $\mathcal{K}_{\rm min}$ is significant for fitting y from the ultracold bosonic molecular collision experiment. For a fermionic system [14,17], the similar calculation can be performed using our model.

IV. CONCLUSION

To summarize, we present a simple theoretical model of arbitrary-order partial-wave scatterings for ultracold molecular collision in the threshold regime. The partial wave and total loss rates as a function of δ^s and y are calculated. The shape resonance plays an important role in the ultracold molecular collision with a very small reactivity. We investigate the effect of shape resonance on molecular collisions. Our analytical theoretical model can give the reasonable result for ultracold bosonic or fermionic molecular collision. As an example of application, the thermally average loss rate for the ^{87}Rb ^{133}Cs + ^{87}Rb ^{133}Cs collision is calculated, and the fitting values of $y = 0.27$ and $\delta^s = 0.62\pi$ are obtained. Moreover, we find an efficient method to fit the loss parameter for ultracold bosonic molecular collision.

ACKNOWLEDGMENTS

We thank Dr. G. Quéméner very much for helpful comments on the paper. This work was supported by the Fundamental Research Funds for the Central Universities Grant No. DUT19LK35, the National Key R&D Program of China (Grant No. 2018YFA0306503), and the National Natural Science Foundation of China under Grant No. 11274056.

APPENDIX: DERIVATION OF THE REFLECTION AND TRANSMISSION COEFFICIENTS

In the long-range region of $R_s \gg 1$, the zero-energy solutions behave asymptotically as

$$\psi_1(R_s) \overset{R_s\gg 1}{=} \frac{(\alpha-2)^{\nu}}{\Gamma(1-\nu)} R_s^{L+1}, \quad \psi_2(R_s) \overset{R_s\gg 1}{=} \frac{(\alpha-2)^{-\nu}}{\Gamma(1+\nu)} R_s^{-L}. \tag{A1}$$

We rewrite Eq. (2) in terms of spherical Bessel functions j_L and n_L as

$$f^{o+} \overset{R_s\gg 1}{=} \frac{e^{i\pi/4}}{\sqrt{\pi k_s}}[ik_sR_sj_L(k_sR_s) - k_sR_sn_L(k_sR_s)]e^{iL\pi/2}, \tag{A2}$$

$$f^{o-} \overset{R_s\gg 1}{=} \frac{e^{i\pi/4}}{\sqrt{\pi k_s}}[-ik_sR_sj_L(k_sR_s) - k_sR_sn_L(k_sR_s)]e^{-iL\pi/2}. \tag{A3}$$

The behavior of $f^{o\pm}$ at large R_s and very low energy, i.e., $k_sR_s \ll 1$, can be expressed by the small-argument expansions of the spherical Bessel functions as [36,37]

$$f^{o+} \underset{k_s\to 0}{\overset{R_s\gg 1}{=}} \frac{e^{i\pi/4}}{\sqrt{\pi k_s}}\left[i\frac{(k_sR_s)^{L+1}}{(2L+1)!!} + \frac{(2L-1)!!}{(k_sR_s)^L}\right]e^{iL\pi/2}, \tag{A4a}$$

$$f^{o-} \underset{k_s\to 0}{\overset{R_s\gg 1}{=}} \frac{e^{i\pi/4}}{\sqrt{\pi k_s}}\left[-i\frac{(k_sR_s)^{L+1}}{(2L+1)!!} + \frac{(2L-1)!!}{(k_sR_s)^L}\right]e^{-iL\pi/2}. \tag{A4b}$$

Substituting Eqs. (A1) and (A4) to Eqs. (4) and (7), we get

$$c_{11}\frac{(\alpha-2)^{\nu}}{\Gamma(1-\nu)}R_s^{L+1} + c_{12}\frac{(\alpha-2)^{-\nu}}{\Gamma(1+\nu)}R_s^{-L} \underset{k_s\to 0}{\overset{R_s\gg 1}{=}} i\frac{e^{i(\pi/4+L\pi/2)}}{\sqrt{\pi k_s}}\frac{k_s^{L+1}}{(2L+1)!!}R_s^{L+1}t^{io} + \frac{e^{i(\pi/4+L\pi/2)}}{\sqrt{\pi k_s}}\frac{(2L-1)!!}{k_s^L}R_s^{-L}t^{io}, \tag{A5}$$

$$c_{21}\frac{(\alpha-2)^{\nu}}{\Gamma(1-\nu)}R_s^{L+1} + c_{22}\frac{(\alpha-2)^{-\nu}}{\Gamma(1+\nu)}R_s^{-L} \underset{k_s\to 0}{\overset{R_s\gg 1}{=}} \frac{e^{i\pi/4}}{\sqrt{\pi k_s}}\left[\frac{i(e^{iL\pi/2}r^{oi} - e^{-iL\pi/2})k_s^{L+1}}{(2L+1)!!}R_s^{L+1} + \frac{(2L-1)!!(e^{iL\pi/2}r^{oi} + e^{-iL\pi/2})}{k_s^L}R_s^{-L}\right]. \tag{A6}$$

Comparing the terms of R_s^{L+1} and R_s^{-L}, respectively, on two sides of the equations, we get

$$c_{11}\frac{(\alpha-2)^{\nu}}{\Gamma(1-\nu)} = i\frac{e^{i(\pi/4+L\pi/2)}}{\sqrt{\pi k_s}}\frac{k_s^{L+1}}{(2L+1)!!}t^{io}, \tag{A7}$$

$$c_{12}\frac{(\alpha-2)^{-\nu}}{\Gamma(1+\nu)} = \frac{e^{i(\pi/4+L\pi/2)}}{\sqrt{\pi k_s}}\frac{(2L-1)!!}{k_s^L}t^{io}, \tag{A8}$$

$$c_{21}\frac{(\alpha-2)^{\nu}}{\Gamma(1-\nu)} = i\frac{e^{i\pi/4}}{\sqrt{\pi k_s}}\frac{(e^{iL\pi/2}r^{oi} - e^{-iL\pi/2})k_s^{L+1}}{(2L+1)!!}, \tag{A9}$$

$$c_{22}\frac{(\alpha-2)^{-\nu}}{\Gamma(1+\nu)} = \frac{e^{i\pi/4}}{\sqrt{\pi k_s}}\frac{(2L-1)!!(e^{iL\pi/2}r^{oi} + e^{-iL\pi/2})}{k_s^L}. \tag{A10}$$

Thus, $f(k_s)$ in Eq. (11) can be extracted from c_{11}/c_{12}.

In the short-range region of $R_s \ll 1$, the zero-energy solutions behave as

$$\psi_1(R_s) \overset{R_s\ll 1}{=} \sqrt{\frac{2R_s}{\pi z}}\cos\left(z - \frac{\pi}{4} + \frac{\nu\pi}{2}\right), \quad \psi_2(R_s) \overset{R_s\ll 1}{=} \sqrt{\frac{2R_s}{\pi z}}\cos\left(z - \frac{\pi}{4} - \frac{\nu\pi}{2}\right). \tag{A11}$$

As low-energy E is negligible compared with the deep potential well in the short-range region, Eq. (3) can be written as

$$f^{i+} = \frac{e^{i\pi/4}}{\sqrt{\pi}}R_s^{\alpha/4}e^{i(z_m-z)}, \tag{A12a}$$

$$f^{i-} = \frac{e^{i\pi/4}}{\sqrt{\pi}}R_s^{\alpha/4}e^{i(z-z_m)}. \tag{A12b}$$

Substituting Eqs. (A11) and (A12) to Eqs. (5) and (7), we get

$$\begin{aligned} &c_{11}\sqrt{\frac{\alpha-2}{\pi}}R_s^{\alpha/4}\cos\left(z - \frac{\pi}{4} + \frac{\nu\pi}{2}\right) + c_{12}\sqrt{\frac{\alpha-2}{\pi}}R_s^{\alpha/4}\cos\left(z - \frac{\pi}{4} - \frac{\nu\pi}{2}\right) \overset{R_s\ll 1}{=} \frac{e^{i\pi/4}}{\sqrt{\pi}}R_s^{\alpha/4}e^{i(z_m-z)} + r^{io}\frac{e^{i\pi/4}}{\sqrt{\pi}}R_s^{\alpha/4}e^{i(z-z_m)}, \\ &\times [c_{21}e^{i(z_m-\pi/4+\nu\pi/2)} + c_{22}e^{i(z_m-\pi/4-\nu\pi/2)}]e^{i(z-z_m)} + [c_{21}e^{-i(z_m-\pi/4+\nu\pi/2)} + c_{22}e^{-i(z_m-\pi/4-\nu\pi/2)}]e^{-i(z-z_m)} \\ &\overset{R_s\ll 1}{=} \frac{2t^{oi}e^{i\pi/4}e^{i(z-z_m)}}{\sqrt{\alpha-2}}. \end{aligned} \tag{A13}$$

Comparing the terms of $e^{i(z-z_m)}$ and $e^{-i(z-z_m)}$, respectively, on two sides of the equations, we finally obtain Eqs. (8)–(10) and the matrix **C** with the elements,

$$c_{11} = \frac{2e^{i\pi/4}}{\sqrt{\alpha-2}} \frac{f(k_s)}{f(k_s)e^{-i(z_m-\pi/4+\nu\pi/2)} + e^{-i(z_m-\pi/4-\nu\pi/2)}}, \quad c_{12} = \frac{2e^{i\pi/4}}{\sqrt{\alpha-2}} \frac{1}{f(k_s)e^{-i(z_m-\pi/4+\nu\pi/2)} + e^{-i(z_m-\pi/4-\nu\pi/2)}},$$
$$c_{21} = -i\frac{2e^{i\pi/4}}{\sqrt{\pi k_s}} \frac{\Gamma(1-\nu)k_s^{L+1}}{(\alpha-2)^{\nu}(2L+1)!!} \frac{e^{i(\nu\pi-L\pi/2)}}{f(k_s)+e^{i\nu\pi}}, \quad c_{22} = i\frac{2e^{i\pi/4}}{\sqrt{\pi k_s}} \frac{\Gamma(1-\nu)k_s^{L+1}}{(\alpha-2)^{\nu}(2L+1)!!} \frac{e^{-iL\pi/2}}{f(k_s)+e^{i\nu\pi}}. \tag{A14}$$

[1] G. Quéméner and P. S. Julienne, Chem. Rev. **112**, 4949 (2012).
[2] R. V. Krems, Phys. Chem. Chem. Phys. **10**, 4079 (2008).
[3] J. Weiner, V. S. Bagnato, S. Zilio, and P. S. Julienne, Rev. Mod. Phys. **71**, 1 (1999).
[4] S. Giorgini, L. P. Pitaevskii, and S. Stringari, Rev. Mod. Phys. **80**, 1215 (2008).
[5] C. H. Greene, P. Giannakeas, and J. Pérez-Ríos, Rev. Mod. Phys. **89**, 035006 (2017).
[6] Y. Ding, J. P. D'Incao, and C. H. Greene, Phys. Rev. A **95**, 022709 (2017).
[7] M. Guo, Xin Ye, J. He, G. Quéméner, and D. Wang, Phys. Rev. A **97**, 020501(R) (2018).
[8] T. Köhler, K. Göral, and P. S. Julienne, Rev. Mod. Phys. **78**, 1311 (2006).
[9] A. Ciamei, A. Bayerle, C.-C. Chen, B. Pasquiou, and F. Schreck, Phys. Rev. A **96**, 013406 (2017).
[10] M. Guo, B. Zhu, B. Lu, X. Ye, F. Wang, R. Vexiau, N. Bouloufa-Maafa, G. Quéméner, O. Dulieu, and D. Wang, Phys. Rev. Lett. **116**, 205303 (2016).
[11] J. Banerjee, D. Rahmlow, R. Carollo, M. Bellos, E. E. Eyler, P. L. Gould, and W. C. Stwalley, Phys. Rev. A **86**, 053428 (2012).
[12] Y. Liu, T. Gong, Z. Ji, G.-R. Wang, Y. Zhao, L. Xiao, and S. Jia, J. Chem. Phys. **151**, 084303 (2019).
[13] J. Rui, H. Yang, L. Liu, D.-C. Zhang, Y.-X. Liu, J. Nan, Y.-A. Chen, B. Zhao, and J.-W. Pan, Nat. Phys. **13**, 699 (2017).
[14] M.-G. Hu, Y. Liu, D. D. Grimes, Y.-W. Lin, A. H. Gheorghe, R. Vexiau, N. Bouloufa-Maafa, O. Dulieu, T. Rosenband, and K.-K. Ni, Science **366**, 1111 (2019).
[15] M. Morita, R. V. Krems, and T. V. Tscherbul, Phys. Rev. Lett. **123**, 013401 (2019).
[16] J.-L. Li and S.-L. Cong, Phys. Rev. A **99**, 022708 (2019).
[17] S. Ospelkaus, K.-K. Ni, D. Wang, M. H. G. de Miranda, B. Neyenhuis, G. Quéméner, P. S. Julienne, J. L. Bohn, D. S. Jin, and J. Ye, Science **327**, 853 (2010).
[18] Y.-X. Liu, J. Nan, D.-C. Zhang, L. Liu, H. Yang, J. Rui, B. Zhao, and J.-W. Pan, Phys. Rev. A **100**, 032706 (2019).
[19] R. Vexiau, J.-M. Launay, and A. Simoni, Phys. Rev. A **100**, 012704 (2019).
[20] D. K. Hoffmann, T. Paintner, W. Limmer, D. S. Petrov, and J. H. Denschlag, Nat. Commun. **9**, 5244 (2018).
[21] M. Mayle, B. P. Ruzic, and J. L. Bohn, Phys. Rev. A **85**, 062712 (2012).
[22] A. Christianen, T. Karman, and G. C. Groenenboom, Phys. Rev. A **100**, 032708 (2019).
[23] J. F. E. Croft, N. Balakrishnan, and B. K. Kendrick, Phys. Rev. A **96**, 062707 (2017).
[24] J. F. E. Croft, C. Makrides, M. Li, A. Petrov, B. K. Kendrick, N. Balakrishnan, and S. Kotochigova, Nat. Commun. **8**, 15897 (2017).
[25] M. D. Frye, P. S. Julienne, and J. M. Hutson, New J. Phys. **17**, 045019 (2015).
[26] B. E. Londoño, J. E. Mahecha, E. Luc-Koenig, and A. Crubellier, Phys. Rev. A **82**, 012510 (2010).
[27] H. M. J. M. Boesten, C. C. Tsai, J. R. Gardner, D. J. Heinzen, and B. J. Verhaar, Phys. Rev. A **55**, 636 (1997).
[28] A. Crubellier, R. González-Férez, C. P. Koch, and E. Luc-Koenig, New J. Phys. **17**, 045020 (2015).
[29] K. Sakimoto, Phys. Rev. A **94**, 042701 (2016).
[30] Y.-P. Bai, J.-L. Li, G.-R. Wang, and S.-L. Cong, Phys. Rev. A **100**, 012705 (2019).
[31] X. Ye, M. Guo, M. L. Gonzalez-Martinez, G. Quéméner, and D. Wang, Sci. Adv. **4**, eaaq0083 (2018).
[32] P. D. Gregory, M. D. Frye, J. A. Blackmore, E. M. Bridge, R. Sawant, J. M. Hutson, and S. L. Cornish, Nat. Commun. **10**, 3104 (2019).
[33] B. Gao, Phys. Rev. A **78**, 012702 (2008).
[34] G.-R. Wang, T. Xie, Y. Huang, W. Zhang, and S.-L. Cong, Phys. Rev. A **86**, 062704 (2012).
[35] G.-R. Wang, T. Xie, Y. Huang, and S.-L. Cong, J. Phys. B: At., Mol. Opt. Phys. **46**, 185302 (2013).
[36] B. P. Ruzic, C. H. Greene, and J. L. Bohn, Phys. Rev. A **87**, 032706 (2013).
[37] *Handbook of Mathematical Functions*, edited by M. Abramowitz and I. A. Stegun (National Bureau of Standards, Washington, D.C., 1964).
[38] Here, the hard-core plus $-1/R_s^{\alpha}$ potential is considered. $S^c = -\exp(i2\int_{R_0}^{R_m} k_s dR_s)$ is defined in Ref. [30], where R_0 is the position of the repulsive potential wall. The collision energy and centrifugal barrier potential are negligible at the short-range region, thus, we obtain $S^c = \exp(i2\delta^s)\exp[i2(-z_m + \pi/4)]$ where the short-range phase shift δ^s is related to z_0 as $\delta^s = z_0 + \pi/4$ and $z_0 = 2/(\alpha-2)R_0^{(2-\alpha)/2}$.
[39] Z. Idziaszek and P. S. Julienne, Phys. Rev. Lett. **104**, 113202 (2010).
[40] K. Jachymski, M. Krych, P. S. Julienne, and Z. Idziaszek, Phys. Rev. Lett. **110**, 213202 (2013).
[41] Z. Idziaszek, G. Quéméner, J. L. Bohn, and P. S. Julienne, Phys. Rev. A **82**, 020703(R) (2010).
[42] Z. Idziaszek, K. Jachymski, and P. S. Julienne, New J. Phys. **17**, 035007 (2015).
[43] G. F. Gribakin and V. V. Flambaum, Phys. Rev. A **48**, 546 (1993).
[44] B. Gao, Phys. Rev. Lett. **105**, 263203 (2010).
[45] B. Gao, Phys. Rev. A **62**, 050702(R) (2000).
[46] B. Gao, Phys. Rev. A **64**, 010701(R) (2001).
[47] K. Sakimoto, J. Phys. B: At., Mol. Opt. Phys. **47**, 025201 (2014).